JOURNAL OF MATERIALS RESEARCH AND TECHNOLOGY 2022;19:2799–2809

Available online at www.sciencedirect.com

jmr&t Journal of Materials Research and Technology

journal homepage: www.elsevier.com/locate/jmrt

Original Article

# Low roughness, elevated stiffness and thickness-modulated surface nanocomposites based on the controlled deposition of polystyrene nanoparticles

Mariusz Borkowski [a,b], Łukasz Mazur [b,c], Krzysztof Maćkosz [b,d,e], Tomasz Mazur [b], Michał Szuwarzyński [b,*]

[a] Polish Academy of Sciences, Jerzy Haber Institute of Catalysis and Surface Chemistry, Niezapominajek 8, 30-239, Krakow, Poland

[b] AGH University of Science and Technology, Academic Centre for Materials and Nanotechnology, Mickiewicza 30, 30-059, Krakow, Poland

[c] AGH University of Science and Technology, Faculty of Materials Science and Ceramics, Mickiewicza 30, 30-059, Krakow, Poland

[d] AGH University of Science and Technology, Faculty of Physics and Applied Computer Science, Al. Mickiewicza 30, 30-059, Krakow, Poland

[e] EMPA Swiss Federal Laboratories for Materials Science and Technology, Laboratory for Mechanics of Materials and Nanostructures, Feuerwerkerstrasse 39, CH-3602, Thun, Switzerland

ARTICLE INFO

*Article history:*
Received 28 March 2022
Accepted 6 June 2022
Available online 9 June 2022

*Keywords:*
Polystyrene
Nanoparticles
Coatings
Atomic force microscopy
DMT modulus
Random sequential adsorption (RSA) theory

ABSTRACT

A significant interest in the versatile and controlled fabrication of surface coatings is present nowadays in materials science. Here we present a repeatable and efficient method of obtaining polystyrene (PS) layers based on the use of controlled deposition of polystyrene nanoparticles (PS-NPs) in the strictly defined amount and forming a smooth (RMS below 1 nm) coating by melting them. Due to the dependence between the concentration of the applied nanoparticles and the thickness of the obtained homogeneous layer, it is possible to control the thickness of the PS coating straightforwardly. Moreover, in this technique, the initial solvent is quickly evaporated, which results in coatings with a higher DMT modulus (up to 8 GPa) compared to spin- or dip-coated methods. We have obtained PS layers on silicon, glass, gold and steel substrates and we have shown the application of our method to cover highly-rough patterned surfaces. Finally, our method is time- and cost-effective due to the inclusion of only the simple heating process and no need to use any advanced equipment. The topography and thickness of PS coatings were studied using atomic force microscopy (AFM) and scanning electron microscopy (SEM) and all are in good correlation with the theoretical calculations.



* Corresponding author.
E-mail address: szuwarzy@agh.edu.pl (M. Szuwarzyński).

https://doi.org/10.1016/j.jmrt.2022.06.031

## 1. Introduction

The control over surface coating on different materials is a significant subject in many fields of modern science. This is especially true in novel targeted materials and high-tech industry solutions [1,2]. Due to the simplicity, versatility, scale and costs of the production process, polymer coatings are gaining more and more popularity [3]. Among many deposition techniques of polymers, the most efficient seems to be coating preparation by the spin- [4] or dip-coating [5] treatment using dissolved polymer in organic solvents or the layer-by-layer (LBL) approach [6]. Those types of methods are easy to implement, repeatable and quick. Such an approach to layer production is unfortunately limited by the small area of formed monolayers and difficult control over thickness, roughness and uniformity of the surfaces, qualities most crucial and demanded in many applications [7]. Anticorrosive and passivating protection of metallic surfaces applications can be considered among the most common uses of thin polymer coatings [8,9]. The general protective properties of such systems result not only from the hindered diffusion of corrosion factors, but also from changing the adhesive [10] and wetting [11] properties of the material surface. Moreover, using materials with mixed properties, it is possible to obtain adhesive and photosensitive layers [12,13]. These types of layers are often used as surface media to modify the optical, electrical and tribological properties of solid and bulky materials. Combining the intrinsic properties of unmodified surfaces with additional polymer layer gives rise to new ones: electronic functionality, lightweight, mechanical flexibility and facile solution-processing over large areas [14,15]. Moreover, since the conjugated polymer layers are characterized by low-bandgap energy, they are used in modern photovoltaics, photodetectors, and transistors [16–18]. Another important group of applications of polymeric films is their use for cells biocompatibility in medicine [19], antibacterial surfaces [20], nature-minic coatings [21] and cell culture scaffolds [22]. Polymeric nanocomposites find also their application in the emerging and rapidly developing field of energy-related applications - serving in supercapacitors [23,24], solar cells [25,26], batteries [27–29] or fuel cells [30]. Materials for these purposes are silica, carbon nanotubes, graphene, boron nitride and metal oxides. Another application is sensing, which employs different types of polymers, and does include their stretching, bending, and twisting – which then cause changes in the electrical resistance, current, and/or capacitance of the active material in the composite. Several novel solutions are presented for sensors [31,32] and flexible strain materials, serving in wearable applications [33].

Herein, we present a never-reported approach of using self-assemblies of colloidal polystyrene nanoparticles (PS-NPs) as a precursor for thickness-controlled coatings of surfaces. PS-NPs are commonly used to fabricate 2D colloidal crystals due to their ability to spontaneously form mono-, bi- and multilayer by changing preparation conditions and fabrication methods [34]. Assembled 2D polystyrene nanoparticles could find applications as the templates for bottom-up nanosphere lithography in solar cell studies, optofluidics and nanophotonics [20,35] or as templates for scaffolds of 3D cell culture matrix [36].

The drop-casting method, disregarding its simplicity and low cost makes it difficult to receive large area colloidal PS-NPs monolayers and the applications are limited due to the difficulties with controlling the number of nanoparticles layers [37]. Unfortunately, similar problems with the formation of large areas of monolayer assemblies are characteristic of dip-coating technology. Even though the problem of unwanted aggregation of nanoparticles could be solved by the addition of surfactant, that heterogeneous surface covering and forming cracks remain a challenge to overcome [38]. The spin-coating method is commonly used to fabricate nanoparticle colloidal crystals. In this technique, a suspension of nanoparticles is spread over a rotating substrate. Spin-coating is more useful for multilayers assemblies where the presence of a defect in surface covering is acceptable [39,40]. Of all fabrication methods of high-quality monolayer colloidal crystals, the most promising seems to be the Langmuir-Blodgett method where nanoparticles monolayer is formed on the air-water interface. Even the air-water interface method prepared to realize a large-scale fabrication of two-dimensional colloid monolayer, as a coating fabrication method seems to suffer from a quasi-double layer structure formation [21,23]. Moreover, from the point of view of potential applications as coatings, its application may be limited due to the difficulties with transferring the layer into a solid substrate. In this paper, we decided to use a simple desorption method from nanoparticles suspension to fabricate thickness-controlled coating of surfaces just by using polymer nanoparticles deposition on various substrates. In our experiment, we used the PS-NPs concentration as a controlling parameter for the degree of surface coverage and resulting thickness of the whole polymer layer. According to the random sequential adsorption (RSA) theory [41] the degree of surface coverage by nano-sized spherical objects depends on the dispersion concentration, exposure time, surface potential and particles size, and ionic strength of dispersion [42]. Self-assembled PS-NPs were melted over the phase transition temperature creating a thickness–controlled polystyrene layer. The thermal polymer coating technique is characterized by high repeatability over the entire surface, homogeneity of the layer and low surface roughness. Due to the controllability of polymer film thickness and theoretical prediction of the required degree of surface covered by nanoparticles, the method is highly scalable and suitable for highly dependent coverage patterns. Contrary to the previously described methods, the one presented here favours quickly solvent removal, which leaves coatings with a higher DMT modulus, compared this parameter obtained by standard methods.

## 2. Experimental section

### 2.1. *Materials*

Styrene (containing 4-tert-butylcatechol as a stabilizer, ≥99%), potassium persulfate ($K_2S_2O_8$, ≥99.0%) and poly(-ethyleneimine) (PEI, branched, analytical standard) were

supplied by Sigma Aldrich. All solutions were prepared using ultra-pure water of resistivity 18.2 MΩ cm (Millipore). Silicon wafers used in the experiments were purchased from Siegert Wafer GmbH (Aachen, Germany). Gold surfaces (200 nm of gold on glass) were purchased from Ssens bv (Enschede, The Netherlands). Glass surfaces, standard microscope slides were provided by Equimed (Krakow, Poland). Steel samples were cut from consumer-grade metal packing can (Brzesko-Okocim, Poland). All substrates were thoroughly cleaned - washed in methanol, acetone (Avantor Performance Materials, Poland) and finally in ultra-pure water in an ultrasonic bath for 10 min for each solvent.

### 2.2. Methods

Atomic force microscope (AFM) topography images were obtained with Dimension Icon XR microscope (Bruker, Santa Barbara, CA, USA) working in the air in the PeakForce Tapping (PFT) mode using standard silicon cantilevers of nominal spring constant of 0.4 N/m and triangular geometry tip with a nominal tip radius of 2 nm. Moreover, using PeakForce Tapping Quantitative Nanomechanical Mapping (PF QNM) mode in the air topography with additional modulus, adhesion, indentation channels was gathered [43]. Derjaguin–Muller–Toporov (DMT) [44,45] model was used to determine nanomechanical parameters of the obtained PS coatings and it was chosen by default by Bruker AFM software due to used PF QNM mode. All PF QNM images were obtained with previously calibrated probes with a spring constant specified on 36.52 N/m and a tip radius of 30 nm. To determine the exact values of spring constant and tip radius, all probes were calibrated according to the procedure recommended by the manufacturer and described in the AFM manual. Deflection sensitivity data were obtained by engaging and ramping the probe onto a smooth silica surface, spring constant value was calculated after a thermal tuning process using Lorentzian fit and tip radius was specified on PS calibration sample (spin-coated, modulus of 2.9 GPa). For analysis, 12 different areas were taken for calculations. Roughness (RMS) parameters were averaged from 10 different 5 × 5 μm areas of each sample excluding visible external artifacts. Scanning Electron Microscopy (SEM) images were obtained with Versa 3D (FEI, Hillsboro, OR, USA) microscope at an accelerating voltage of 20 kV. All PS coatings samples were broken in half to reveal the cross-section of the layer. Nanoparticles size and charge were measured with ZetaSizer Nano ZS (Malvern Panalytical) in the configuration for a measurement angle of 173°.

### 2.3. Synthesis of polystyrene nanoparticles (PS-NPs)

Negatively charged sulfate polystyrene nanoparticles (PS-NPs) were synthesized using the emulsifier-free emulsion polymerization of styrene. The mixture of 150 ml of 0.017 M sodium chloride was purged using argon and heated to 70 °C in a glass reactor equipped with a mechanical stirrer and reflux condenser. Next, 11 ml of styrene and, afterward 5 ml of 0.163 M potassium persulfate aqueous solution were added into this mixture. The polymerization reaction was conducted under argon atmosphere at 70 °C for 24 h, mechanical stirring was used. After synthesis, the white suspension was purified two times using centrifugation at 8000 rpm. The final precipitate was redispersed in 100 ml of water to obtain a concentration of 27.0 mg/ml. The measured surface potential of PS-NPs was −34.8 ± 4.4 mV and the average diameter of nanoparticles was 658 ± 38 nm using AFM and 670 ± 45 nm. The latter values were measured by the DLS technique - see Fig. S1 in the Supporting Information.

### 2.4. PS-NPs controlled deposition on surfaces

The silicon, gold, glass and steel surfaces were cleaned in methanol, acetone and finally in ultra-pure water and then dried under a stream of argon. The washed and dried substrates were oxidized in oxygen plasma (Plasma Cleaner PDC-32G-2, exposition time: 15 min, oxygen flow rate: 25 ml/min). Next, the prepared substrates were immersed in polyethyleneimine (PEI, 1 mg/ml) water solution for 15 min to create a positively charged polymer film on the surface (LbL-approach). Monodisperse PS-NPs deposition onto modified positively charge substrate interfaces was carried out by immersion substrates from the previous step in nanoparticles suspension with selected concentration for 25 min (see Scheme 1B). For all surfaces, three different concentrations of PS-NPs were used: 27.00 mg/ml (PS-NPs-0), 2.70 mg/ml (diluted 10 times, PS-NPs-10) and 0.27 mg/ml (diluted 100 times, PS-NPs-100). Moreover for silicon surface three additional solutions were prepared with concentrations of 5.40 mg/ml (diluted 5 times, PS-NPs-1), 1.08 mg/ml (diluted 25 times, PS-NPs-25) and 0.54 mg/ml (diluted 50 times, PS-NPs-50). Finally, deposited surfaces were washed with water and dried under a stream of argon.

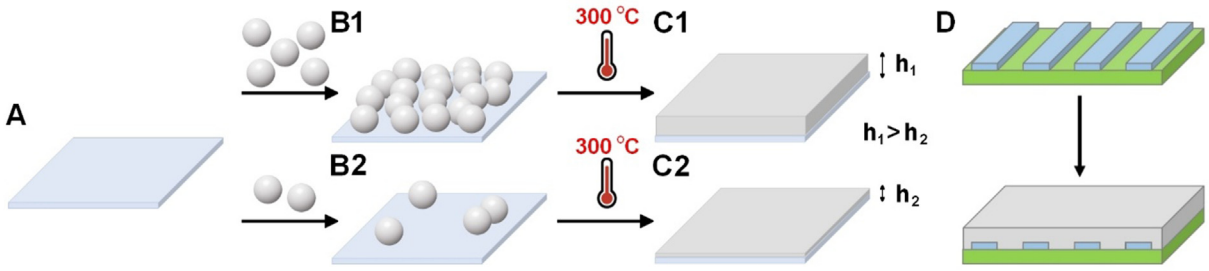


**Scheme 1 – Fabrication of thick (1.) and (2.) thin PS coatings: A. bare substrate (silicon wafers, glass, gold or steel), B. PS nanoparticles deposition, C. controlled melting in 300 °C, D. *facile* coating method on the high-roughness surface.**

### 2.5. *Fabrication of thickness-modulated polystyrene coatings*

Fabrication of polystyrene coatings was carried out by heating on the hot plate PS-NPs deposited on studied surfaces at 300 °C for 10 min (see Scheme 1C). Additionally, the samples were covered with a glass lid to ensure uniform heating of the entire surface.

## 3. Results

### 3.1. *PS-NPs coverage of surfaces*

Following the general concept, we have assumed that we can design a facile, repeatable, and cheap method of coating fabrication allowing for modulated control of layer thickness. Moreover, in our assumption, we wanted to obtain coatings with a uniform coverage even on rough surfaces (see Scheme 1D). Firstly, we investigated controlled deposition on flat silicon wafers (covered with a silicon oxide thin layer). PS-NPs were deposited from solutions of different concentrations, resulting in various surface coverage. For the most concentrated solution of PS-NPs-0 (27 mg/ml), the surface coverage area was 46.09 ± 3.13%. which, is the theoretical limit value of the surface coverage (see Fig. 1A). The measured parameter is close to the literature value, which estimates the maximum surface coverage of charged particles to the theoretical value of 54.7% [46]. The lower obtained values result from differences in the surface charge of negatively charged PS-NPs in relation to the model values [27,32] and higher repulsive forces between individual particles. For all samples, surface coverage parameters were calculated from atomic force microscopy (AFM) data using bearing analysis function with the bearing depth of 330 nm, which is half of the average height of the low-dispersibility spherical nanoparticles (see Fig. 1B1 and 1B2) measured previously using AFM. This value can be counted as the average radius of the nanoparticle and the height at which when viewed from above, the PS-NPs cover the largest area. As mentioned, the measured surface coverage value has reached the limit value, which means that the used concentration was too high. The limiting concentration, where the last time the coverage value

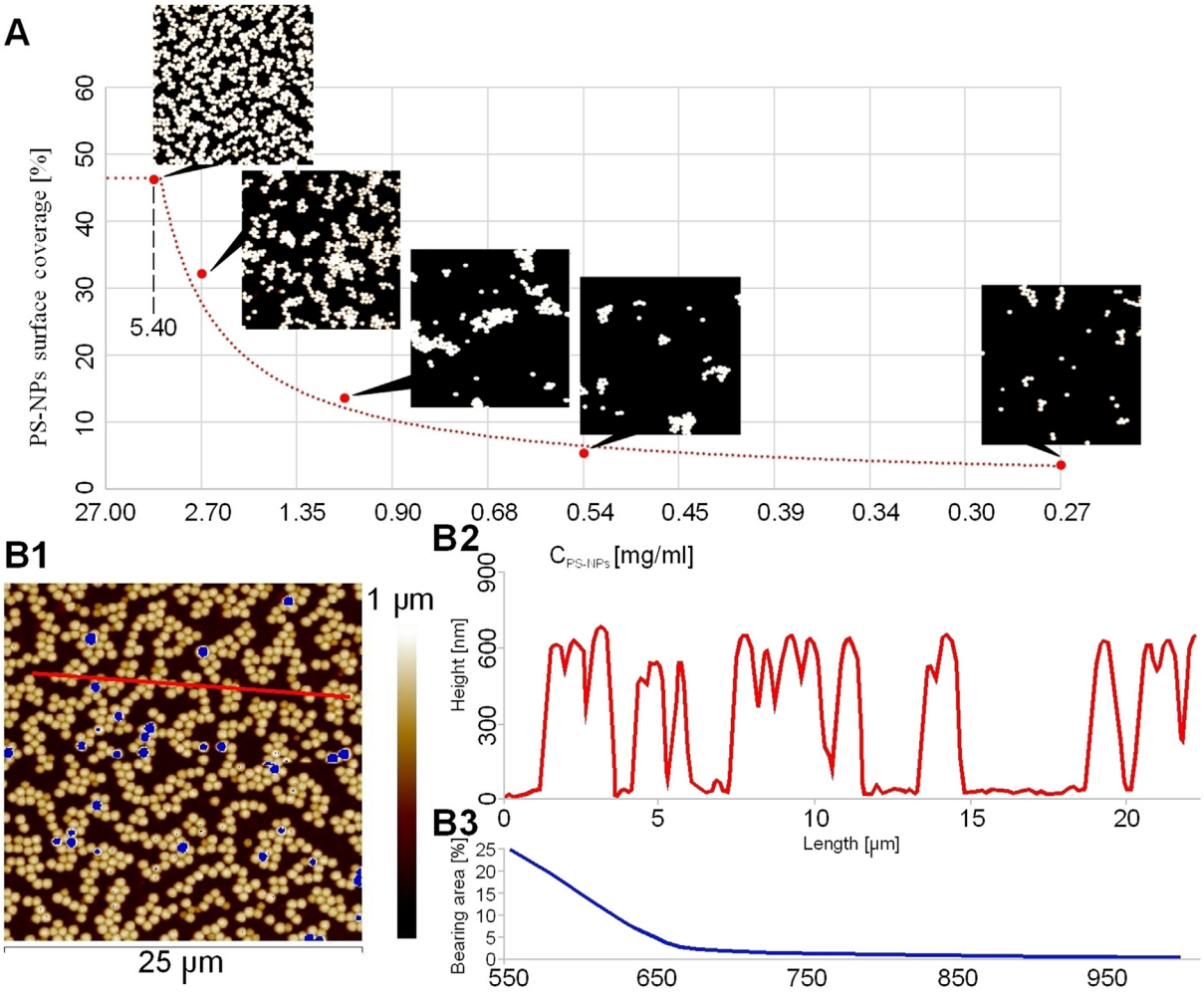


**Fig. 1 – Characterization of silicon surface with adsorbed PS-NPs: A) Surface coverage of PS-NPs desorbed from solutions with different concentrations, B1) AFM image of PS-NPs-1 with corresponding cross-section (B2) and bearing area analysis (B3).**

does not change, was empirically defined to be 5.4 mg/ml (with the coverage of 46.27 ± 2.87%). Further decrease the concentration of the PS-NPs solution led to a controlled reduction of the surface coverage area reaching 32.24 ± 1.07% for PS-NPs-10, 13.64 ± 1.12% for PS-NPs-25, 5.38 ± 0.97% for PS-NPs-50, and 3.57 ± 0.87 for PS-NPs-100, which is shown in Fig. 1A.

The next step was to determine whether the deposition of PS-NPs creates well-defined monolayers. Avoiding aggregates and unwanted stacking of nanoparticles is crucial for the thickness-controlled formation of layers after melting. All additional nanoparticles would disturb the fine tailoring of polystyrene coatings by an uncontrolled increase in the

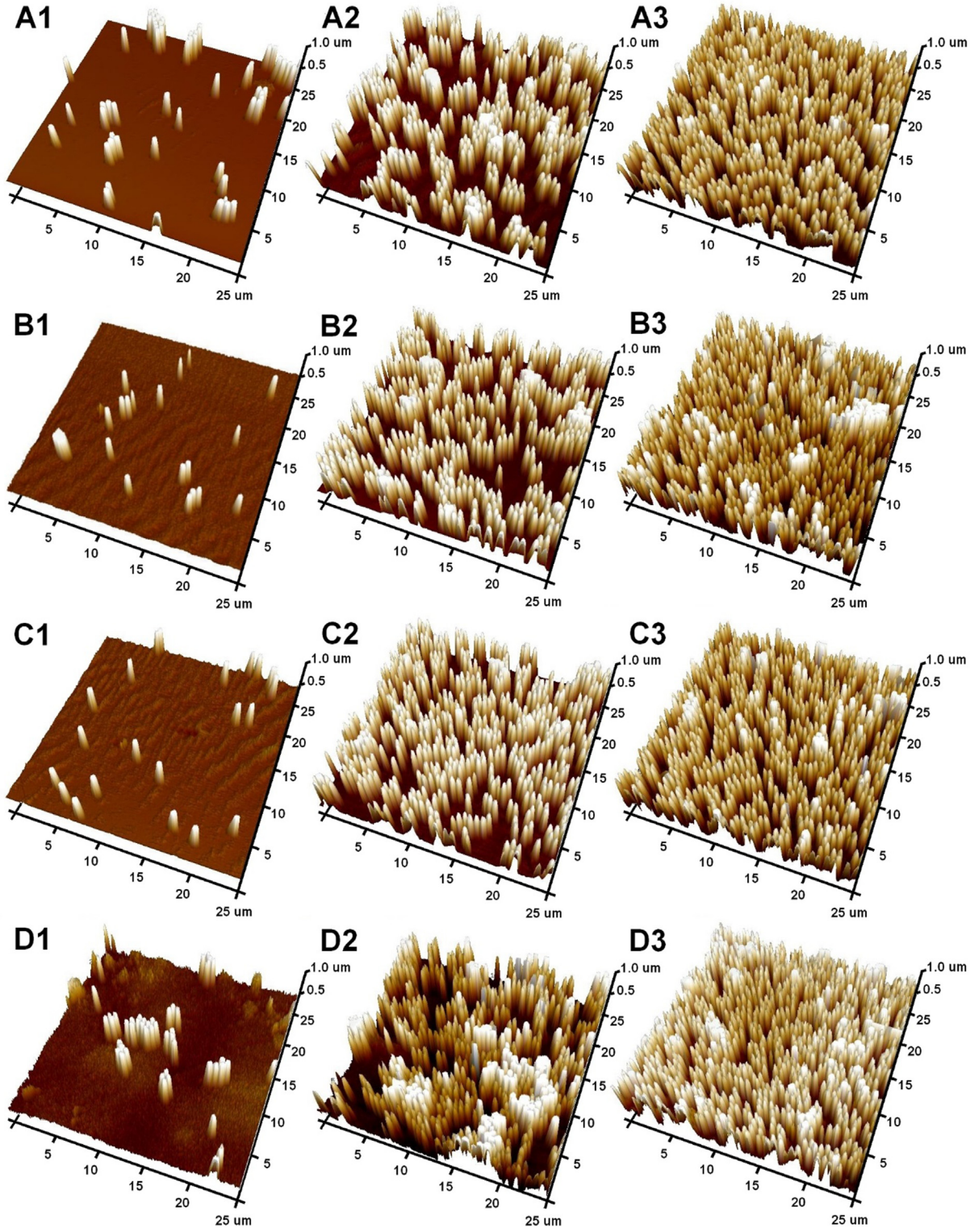


**Fig. 2 – AFM 3-D images of PS-NPs-1 (1), PS-NPs-10 (2), and PS-NPs-100 (3) on silicon (A), glass (B), gold (C), and steel (D).**

thickness of the layer. The AFM technique was used to determine the surface coverage by excess PS-NPs located above the desired monolayer. This time the bearing depth in the bearing analysis function was set at 800 nm. For silicon surface, only 1.44 ± 0.21% for the sample deposited from the most concentrated solution (PS-NPs-1, see Fig. 1B2 and 1B3 and in Supporting Information) and 1.29 ± 0.14% for PS-NPs-10. In the most diluted sample of PS-NPs-100, no aggregates or stacks were observed. All mentioned studies were repeated on glass, gold and steel surfaces. The universality of our method is emphasized by the very similar surface coverage by PS-NPs on all substrates, which is clearly visible on AFM images of PS-NPs on all surfaces presented in Fig. 2. Moreover, PS-NPs on all surfaces create a monolayer deposition with very low excess nanoparticles (up to 4.32 ± 0.47% for steel surface covered from solution with PS-NPs-10). All surface coverage data for PS-NPs mono- and multilayers are gathered in Table 1.

### 3.2. *PS coatings characterization*

Polystyrene layers were obtained by melting deposited PS-NPs on surfaces with no further processing. The thicknesses of PS layers were known by AFM measurements of scratched

**Table 1 – PS-NPs surface coverage of mono- and multilayers with a calculated and measured thickness of polystyrene layer on silicon, glass, gold and steel.**

| Substrate | $C_{PS\text{-}NPs}$ [mg/ml] | PS-NPs surface coverage [%] | PS-NPs multilayer coverage [%] | Thickness of PS layer [μm] | | RMS of PS layer [nm] |
|---|---|---|---|---|---|---|
| | | | | Calculated | Measured | |
| Silicon | 5.40 | 46.27 ± 2.87 | 1.44 ± 0.21 | 0.207 ± 0.013 | 0.218 ± 0.021 | 0.59 ± 0.17 |
| | 2.70 | 32.24 ± 1.07 | 1.29 ± 0.14 | 0.145 ± 0.006 | 0.160 ± 0.012 | 0.62 ± 0.19 |
| | 0.27 | 3.57 ± 0.87 | 0.00 ± 0.00 | 0.015 ± 0.003 | 0.017 ± 0.004 | 0.49 ± 0.09 |
| Glass | 5.40 | 43.17 ± 3.49 | 2.04 ± 0.29 | 0.205 ± 0.016 | 0.213 ± 0.021 | 0.89 ± 0.12 |
| | 2.70 | 34.61 ± 1.88 | 0.88 ± 0.15 | 0.158 ± 0.009 | 0.160 ± 0.012 | 0.77 ± 0.14 |
| | 0.27 | 3.71 ± 1.05 | 0.01 ± 0.00 | 0.016 ± 0.004 | 0.017 ± 0.004 | 0.56 ± 0.11 |
| Gold | 5.40 | 45.34 ± 1.33 | 1.56 ± 0.22 | 0.194 ± 0.007 | 0.201 ± 0.011 | 0.44 ± 0.08 |
| | 2.70 | 35.50 ± 1.69 | 0.35 ± 0.08 | 0.152 ± 0.007 | 0.152 ± 0.012 | 0.50 ± 0.13 |
| | 0.27 | 3.78 ± 0.77 | 0.00 ± 0.00 | 0.016 ± 0.003 | 0.017 ± 0.003 | 0.42 ± 0.10 |
| Steel | 5.40 | 45.23 ± 2.01 | 1.07 ± 0.10 | 0.201 ± 0.009 | 0.193 ± 0.024 | 0.92 ± 0.21 |
| | 2.70 | 34.42 ± 2.07 | 4.32 ± 0.47 | 0.167 ± 0.011 | 0.170 ± 0.021 | 0.81 ± 0.13 |
| | 0.27 | 3.30 ± 0.86 | 0.00 ± 0.00 | 0.014 ± 0.004 | 0.019 ± 0.004 | 0.67 ± 0.14 |

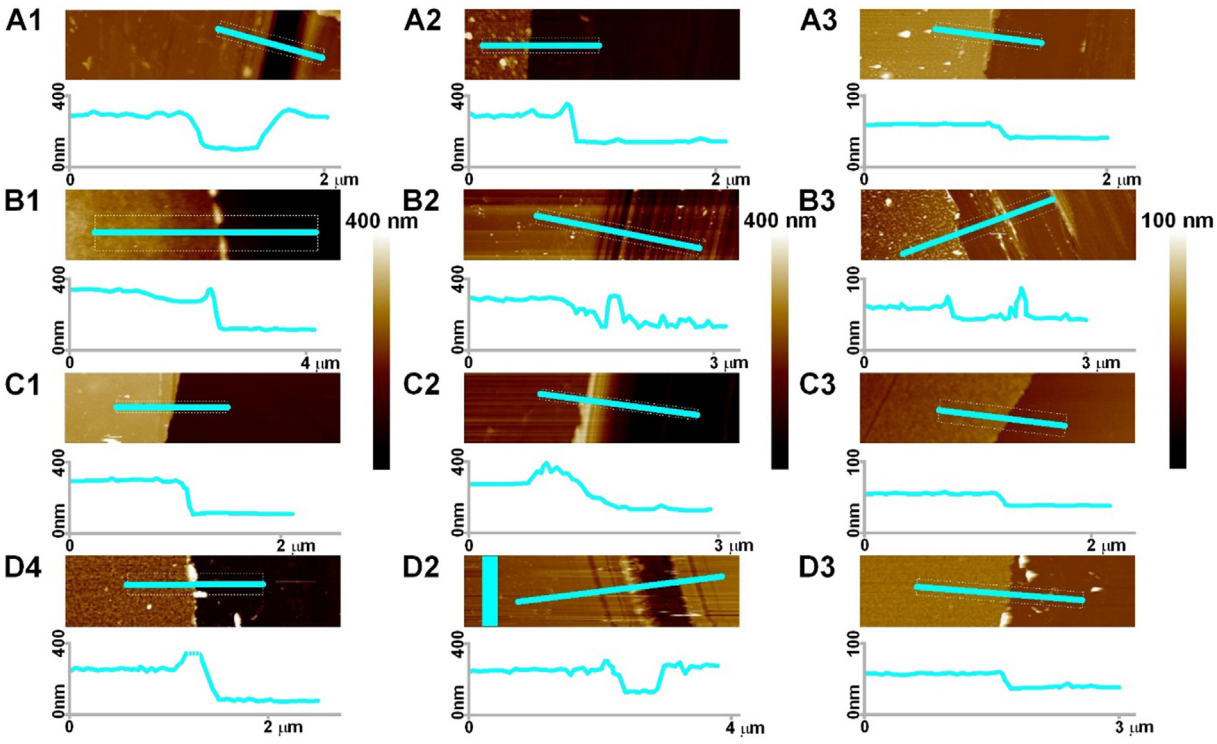


**Fig. 3 – AFM characteristic of polystyrene coatings on silicon (A), glass (B), gold (C), and steel (D) obtained from PS-NPs-1 (1), PS-NPs-10 (2) and PS-NPs-100 (3).**

surfaces. These measurements confirmed our initial assumption of obtaining a facile, efficient and surface-independent method of coating substrates and controlling the resulting thickness. It seems that the thickness of PS layers depends not on the type of the surface, but on the total number of PS-NPs (as the surface coverage area of deposited PS-NPs). For silicon, glass, gold and steel substrates, obtained results, presented in Fig. 3, are similar to each other and lays in the range of 17–19 nm for PS-NPs-100, 152–170 nm for PS-NPs-10 up to 193–218 nm for PS-NPs-1 (see Table 1). Significant differences in the thickness of the layers obtained from the samples were confirmed using scanning electron microscopy (SEM) – see Fig. S3 and paragraph 4 in Supporting Information. As with AFM, the thickest layer is the observed layer for PS-NPs-1 deposition, while the thinnest for PS-NP-100. Moreover, all measured thicknesses are in good agreement with theoretical calculations. Theoretical parameters (Table 1, Table S1 and S2 in the Supporting Information) were calculated using surface coverage data from AFM bearing analysis function and some basic equations, which are described in detail in paragraph 3 in the Supporting Information. All experimental and theoretical data for surfaces have been compared to each other. As it is presented in Fig. 4 measured and theoretically calculated thicknesses for all PS layers are in good correlation. Moreover, the PS-NPs area coverage on all surfaces corresponds to the thickness of the obtained layers, which clearly confirms the facile modularity of this method. Another undeniable advantage of the presented method is the obtained coatings low roughness (RMS). For all thicknesses and all surfaces, RMS parameters are below 1 nm, which is in good correlation to the RMS parameters for the spin-coated polystyrene layer on the AFM calibration sample (0.42 ± 0.12 nm). All RMS data are gathered in Table 1.

### 3.3. *Nanomechanical characterization of PS layers*

The method of fabrication of PS coatings relies on the direct deposition of PS-NPs from an aqueous solution. Desorbed and electrostatically organized (attractive interactions between positively charged surface and negatively charged nanoparticles, repulsive interactions between uniformly charged PS-NPs) are melted in 300 °C. Such high temperature causes water to drain off very quickly and the dry nanoparticles can start the melting process without the presence of a solvent. Moreover, melted clear polystyrene was left at the set temperature for 10 min. All those methods should make forming a PS solidifying layer harder than layers obtained in quicker processes and from solvent solutions (i.e., spin coating, dip coating). Using AFM working in the PFT Quantitative Nanomechanical Mapping (PF QNM) mode we have determined nanomechanical parameters of the obtained PS coatings on the silicon, glass, gold and steel surfaces and additionally on spin-coated PS layer on silicon and an identical spin-coated sample but from an AFM calibration kit (see Fig. 5). All

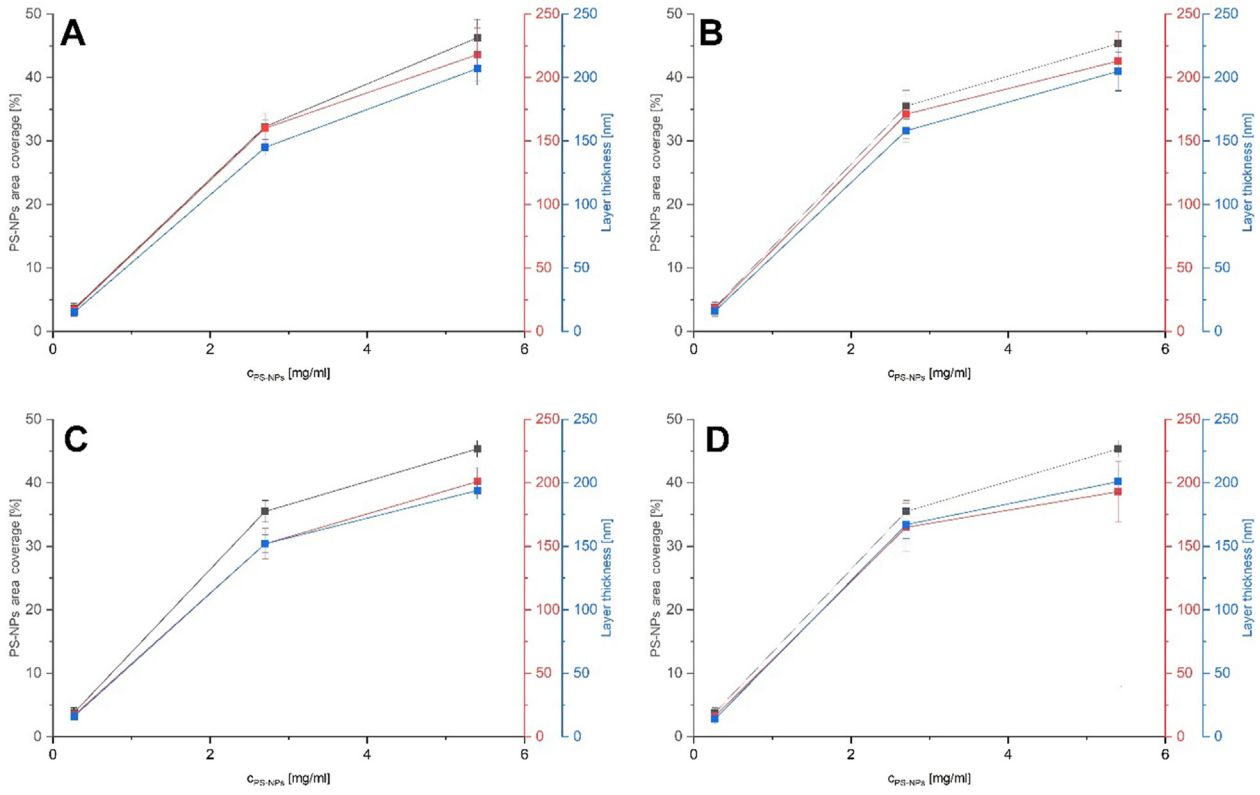


**Fig. 4 – Plots of PS-NPs surface area coverage and related theoretical and measured thickness of PS layer after melting in the terms of concentration of deposited PS-NPs on surfaces: A) silicon, B) Glass, C) Gold, D) Steel. Black plots correspond to the PS-NPs surface area coverage, blue plots to the theoretical thickness and red plots to the measured thickness.**

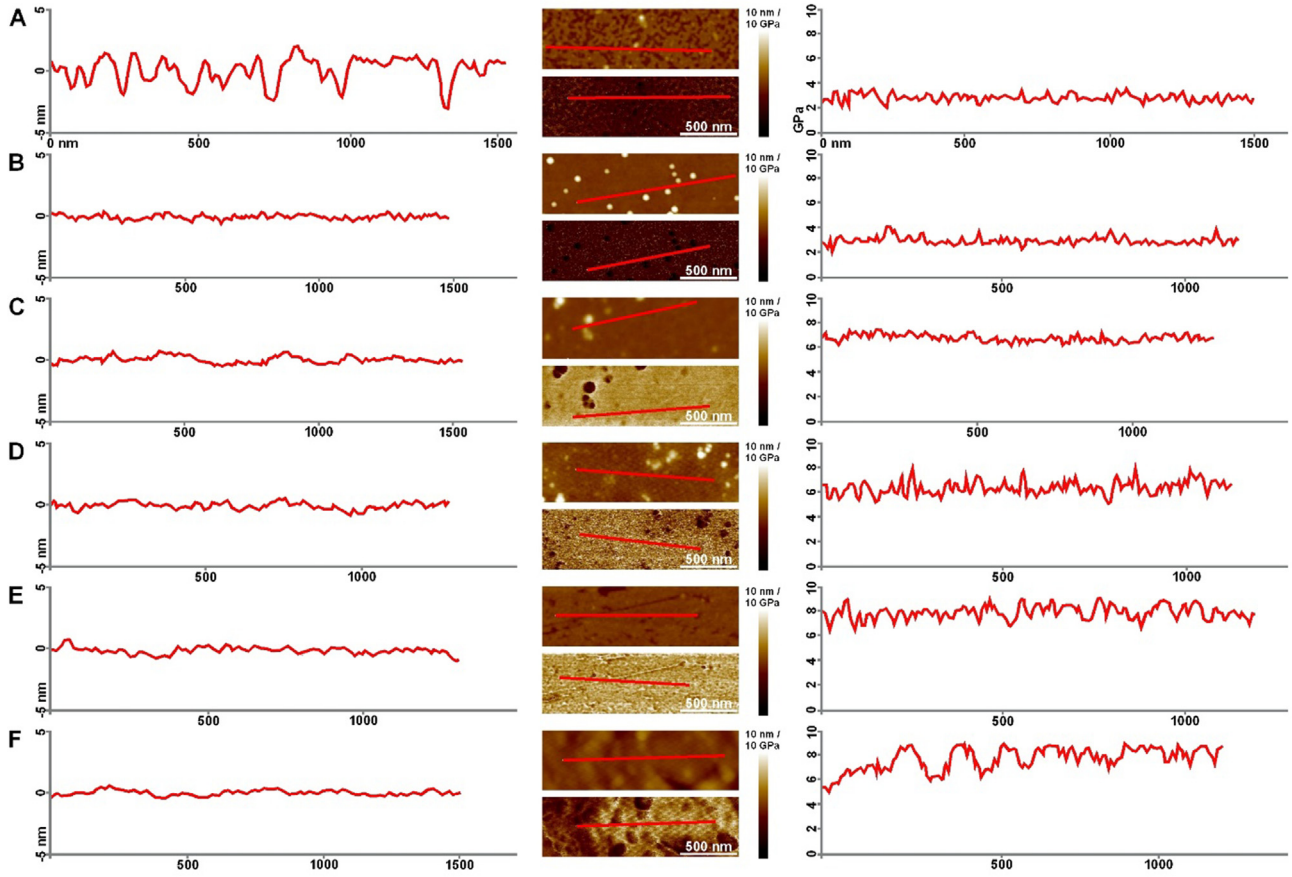


**Fig. 5 – AFM topography (top) and DMT modulus (bottom) images with corresponding topography (left) and DMT modulus (right) cross-sections obtained in PF QNM for PS samples: A) spin-coated on silicon, B) spin-coated on silicon from AFM calibration kit, C) melted coating on silicon, D) melted coating on glass, E) melted coating on gold, F) melted coating on steel.**

moduli of the samples were obtained from the Derjaguin–Muller–Toporov (DMT) model after the previous calibration of measuring probes. DMT modulus for spin-coated sample on silicon (3.08 ± 0.21 GPa) was equal to the literature data (3.0 GPa – for thick PS spin-coated layers, 3.4 GPa for dip-coated layers and 3.0–3.5 GPa for bulk materials) [47,48]. Moreover, the measured result is consistent with the results of the spin-coated PS sample on silicon from the AFM calibration

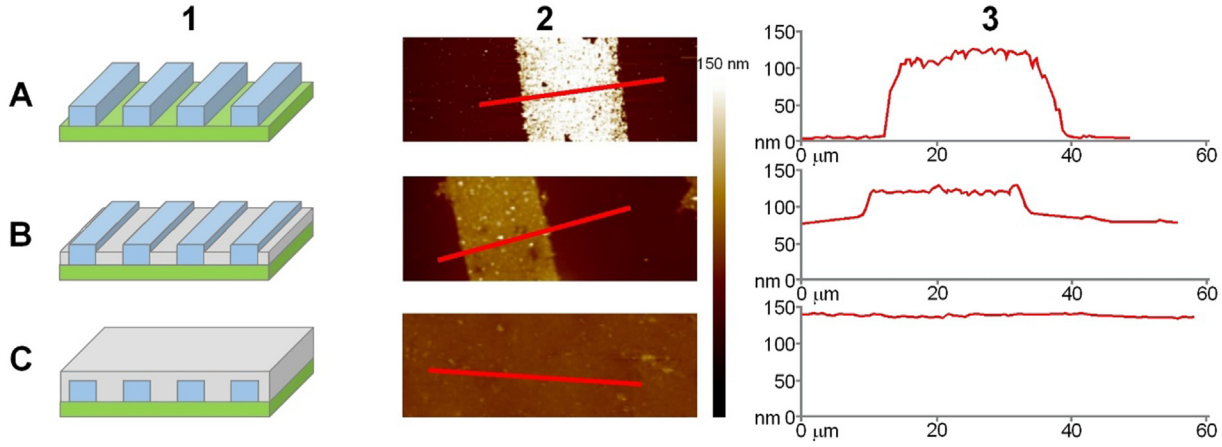


**Fig. 6 – Thickness-modulated PS coatings on silver patterned stripes on silicon: bare stripes (A), stripes partially covered with coating obtained from PS-NPs with c = 1.10 mg/ml (B) and stripes fully covered with coating obtained from PS-NPs with c = 5.4 mg/ml (C); (1) Schematic drawing, (2) AFM topography image and (3) AFM cross-section.**

kit (2.92 ± 0.10 GPa). Measured DMT modulus for PS-NPs-1 melted coating on silicon is more than two times higher (7.03 ± 0.17 GPa) than the spin-coated one. DMT modulus for all PS melted layers is similar on each type of surface, however, the visible difference is in the homogeneity of the coating surfaces presented in the rise of RMS parameters of the DMT data. The measured DMT modulus for glass is 6.97 ± 0.34 GPa, for gold is 7.95 ± 0.39 GPa and for steel is 8.14 ± 0.81 GPa. The performed PF QNM measurements confirmed our assumptions that our PS-NPs melting method without the presence of a solvent significantly increases the modulus of the obtained layers, which can be used as protective and insulating coatings.

### 3.4. *High-roughness surfaces covering studies*

In the last characterization, we did we decided to confirm the possibility of covering a non-flat surface with a layer of demanded thickness. Therefore, we covered surfaces of previously obtained patterned high-roughness silver stripes with a width of 25 μm and a thickness of 118 ± 9 nm (see Fig. 6A). In our assumption, by controlling the amount of PS-NPs, we will be able to partially and completely cover the silver stripes. According to the previous results, shown in Fig. 4, we chose the concentrations of PS-NPs solutions for 1.10 mg/ml for partial coverage in the level of two-third parts and 5.51 mg/ml for the complete coverage. As it is presented in Fig. 6B the fabricated PS layer filled the spaces between the silver stripes to a thickness of 65–74% of the total height of the strip. The usage of higher concentration results in complete coverage of the stripes (see Fig. 6C), which makes both of our estimations correct.

## 4. Conclusions

The results, presented above, support the hypothesis that monolayer deposition of polystyrene nanoparticles and melting them at 300 °C could serve as a well-controlled and efficient method of fabrication of thickness-modulated polymer coatings. The presented method does not require the usage of any advanced laboratory equipment, time-consuming experiments and tedious cleaning processes. The only thing needed is a hot plate, which makes the fabrication process very low cost. Moreover, the presented method can be applied on many different surfaces (silicon, glass, gold, steel) achieving similar unified parameters of coverage (thickness, roughness, DMT modulus). Based on the measurements and theoretical calculations, the thickness of PS layers can be tailored in the range of single nanometers up to several hundred nanometers. In presented examples, the 218 ± 21 nm thick PS layer was achieved from a nanoparticle concentration of 5.4 mg/ml, which corresponded to the most densely packed PS-NPs monolayer on the surface. The surface coverage can not be higher because of repulsive interactions between uniformly charged nanoparticles forming monolayer before the melting process, which follows directly from the random sequential adsorption (RSA) theory. AFM working in PF QNM mode confirmed high modulus of PS coatings: 7.03 ± 0.17 GPa for silicon, 6.97 ± 0.34 GPa for glass, 7.95 ± 0.39 GPa for gold and 8.14 ± 0.81 GPa for steel substrate. Obtained values are around 2.5 times higher for the spin- or dip-coated and bulk samples (2.9–3.5 GPa), which is caused by solidifying process of melted PS without the presence of any solvent, that would need to be vaporized. Finally, we applied our method to cover high-roughness surfaces with a layer of demanded thickness in a controlled way. We proved that the calculated concentration of nanoparticles deposited to the non-smooth surface is in good relation with experimental data and will flatten the rough surface with a high yield for both partial and full coverage. The experimental simplicity of our method makes the controlled PS-NPs melting technique a good candidate as a facile and scalable alternative for the common techniques such as spin- or dip-coating and a novel approach in obtaining elevated modulus polystyrene coatings keeping low roughness of the layers (RMS < 1 nm).

## Data availability statement

The raw/processed data required to reproduce the findings of this study are available on request from the corresponding author [szuwarzy@agh.edu.pl].

## Authorship contribution statement

**M. Borkowski:** Conceptualization, Methodology, Writing – original draft. **Ł. Mazur:** Methodology. **K. Maćkosz:** Methodology. **T. Mazur:** Methodology, Writing – review & editing. **M. Szuwarzyński:** Conceptualization, Methodology, Writing – original draft, Writing – review & editing.

## Declaration of Competing Interest

The authors declare that they have no known competing financial interests or personal relationships that could have appeared to influence the work reported in this paper.

## Acknowledgment

The authors would like to thank for the financial support to the National Science Centre (Sonata Grant no. 2018/31/D/ST5/02813).

## Appendix A. Supplementary data

Supplementary data to this article can be found online at https://doi.org/10.1016/j.jmrt.2022.06.031.

## REFERENCES

[1] Fotovvati B, Namdari N, Dehghanghadikolaei A. On coating techniques for surface protection: a review. J. Manuf. Mater. Process. 2019;3:28. https://doi.org/10.3390/jmmp3010028.

[2] Kang S, You I, Cho W, Shon H, Lee T, Choi I, et al. One-step modification of superhydrophobic surfaces by a mussel-inspired polymer coating. Angew Chem Int Ed 2010;49:9401–4. https://doi.org/10.1002/anie.201004693.
[3] Kang M-H, Cheon K-H, Jo K-I, Ahn J-H, Kim H-E, Jung H-D, et al. An asymmetric surface coating strategy for improved corrosion resistance and vascular compatibility of magnesium alloy stents. Mater Des 2020;196:109182. https://doi.org/10.1016/j.matdes.2020.109182.
[4] Yin Z, Tian B, Zhu Q, Duan C. Characterization and application of PVDF and its copolymer films prepared by spin-coating and Langmuir–blodgett method. Polymers 2019;11:2033. https://doi.org/10.3390/polym11122033.
[5] Wu X, Wyman I, Zhang G, Lin J, Liu Z, Wang Y, et al. Preparation of superamphiphobic polymer-based coatings via spray- and dip-coating strategies. Prog Org Coating 2016;90:463–71. https://doi.org/10.1016/j.porgcoat.2015.08.008.
[6] Ciejka J, Grzybala M, Gut A, Szuwarzynski M, Pyrc K, Nowakowska M, et al. Tuning the surface properties of poly(allylamine hydrochloride)-based multilayer films. Materials 2021;14:2361. https://doi.org/10.3390/ma14092361.
[7] Park B, Yeong Na S, Bae I-G. Uniform two-dimensional crystals of polystyrene nanospheres fabricated by a surfactantassisted spin-coating method with polyoxyethylene tridecyl ether. Sci Rep 2019;9:11453. https://doi.org/10.1038/s41598-019-47990-z.
[8] Luckachan GE, Mittal V. Anti-corrosion behavior of layer by layer coatings of cross-linked chitosan and poly(vinyl butyral) on carbon steel. Cellulose 2015;22:3275–90. https://doi.org/10.1007/s10570-015-0711-2.
[9] Huang YC, Lo TY, Chao CG, Whang WT. Anti-corrosion characteristics of polyimide/h-boron nitride composite films with different polymer configurations. Surf Coat Technol 2014;260:113–7. https://doi.org/10.1016/j.surfcoat.2014.09.043.
[10] Bleiker SJ, Dubois V, Schröder S, Stemme G, Niklaus F. Adhesive wafer bonding with ultra-thin intermediate polymer layers. Sens Actuators, A 2017;260:16–23. https://doi.org/10.1016/j.sna.2017.04.018.
[11] Yan C, Kim K, Lee S, Bae S, Hong B, Kim J, et al. Mechanical and environmental stability of polymer thin-film-coated graphene. ACS Nano 2012;6:2096–103. https://doi.org/10.1021/nn203923n.
[12] Wang G, Chen C, Chen Y, Kang X, Yang PC, Wang F, et al. Self-stabilized and strongly adhesive supramolecular polymer protective layer enables ultrahigh-rate and large-capacity lithium-metal anode. Angew Chem Int Ed 2020;59:1055–2060. https://doi.org/10.1002/anie.201913351.
[13] Wolski K, Szuwarzyński M, Kopeć M, Zapotoczny S. Ordered photo-and electroactive thin polymer layers. Eur Polym J 2015;65:155–70. https://doi.org/10.1016/j.eurpolymj.2015.01.031.
[14] Lu L, Zheng T, Wu Q, Schneider A, Zhao D, Yu L. Recent advances in bulk heterojunction polymer solar cells. Chem Rev 2015;115:12666–731. https://doi.org/10.1021/acs.chemrev.5b00098.
[15] Huang Y, Kramer EJ, Heeger AJ, Bazan GC. Bulk heterojunction solar cells: morphology and performance relationships. Chem Rev 2014;114:7006–43. https://doi.org/10.1021/cr400353v.
[16] Dou L, Liu Y, Hong Z, Li G, Yang Y. Low-bandgap near-IR conjugated polymers/molecules for organic electronics. Chem Rev 2015;115:12633–65. https://doi.org/10.1021/acs.chemrev.5b00165.
[17] Szuwarzyński M, Wolski K, Kruk T, Zapotoczny S. Macromolecular strategies for transporting electrons and excitation energy in ordered polymer layers. Prog Polym Sci 2021;121:101433. https://doi.org/10.1016/j.progpolymsci.2021.101433.
[18] Al-Muntaser AA, Abdelghany AM, Abdelrazek EM, Elshahawy AG. Enhancement of optical and electrical properties of PVC/PMMA blend films doped with Li4Ti5O12 nanoparticles. J Mater Res Technol 2020;9:789–97. https://doi.org/10.1016/j.jmrt.2019.11.019.
[19] Abdal-hay A, Dewidar M, Lim JK. Biocorrosion behavior and cell viability of adhesive polymer coated magnesium based alloys for medical implants. Appl Surf Sci 2012;261:536–46. https://doi.org/10.1016/j.apsusc.2012.08.051.
[20] Abd El-Kader MFH, Elabbasy MT, Ahmed MK, Menazea AA. Structural, morphological features, and antibacterial behavior of PVA/PVP polymeric blends doped with silver nanoparticles via pulsed laser ablation. J Mater Res Technol 2021;13:291–300. https://doi.org/10.1016/j.jmrt.2021.04.055.
[21] Fiejdasz S, Gilarska A, Horak W, Radziszewska A, Strączek T, Szuwarzyński M, et al. Structurally stable hybrid megnetic materials based on natural polymers – preparation and characterization. J Mater Res Technol 2021;15:3149–60. https://doi.org/10.1016/j.jmrt.2021.09.124.
[22] Górka-Kumik W, Garbacz P, Lachowicz D, Dąbczyński P, Zapotoczny S, Szuwarzyński M. Tailoring cellular microenvironments using scaffolds based on magnetically-responsive polymer brushes. J Mater Chem B 2020;8:10172–81. https://doi.org/10.1039/D0TB01853H.
[23] Reina M, Scalia A, Auxilia G, Fontana M, Bella F, Ferrero S, et al. Boosting electric double layer capacitance in laser-induced graphene-based supercapacitors. Adv. Sustainable Syst. 2022;6:2100228. https://doi.org/10.1002/adsu.202100228.
[24] Chakrabort S, Amal Raj M, Mary NL. Biocompatible supercapacitor electrodes using green synthesised ZnO/Polymer nanocomposites for efficient energy storage applications. J Energy Storage 2020;28:101275. https://doi.org/10.1016/j.est.2020.101275.
[25] Zhu J, Yang X, Yang Z, Wang D, Gao P, Ye J. Achieving a record fill factor for silicon–organic hybrid heterojunction solar cells by using a full-area metal polymer nanocomposite top electrode. Adv Funct Mater 2018;28:1705425. https://doi.org/10.1002/adfm.201705425.
[26] Rahman NA, Hanifah SA, Mobarak NN, Ahmad A, Ludin N,A, Bella F, et al. Chitosan as a paradigm for biopolymer electrolytes in solid-state dye-sensitised solar cells. Polymer 2021;230:124092. https://doi.org/10.1016/j.polymer.2021.124092.
[27] Chen X, Zhao Y, Li L, Wang Y, Wang J, Xiong J, et al. MXene/polymer nanocomposites: preparation, properties, and applications, polym. Rev 2021;61:80–115. https://doi.org/10.1080/15583724.2020.1729179.
[28] Abdah MAAM, Mokhtar M, Khoon LT, Sopian K, Dzulkurnain NA, Ahmad A, et al. Synthesis and electrochemical characterizations of poly(3,4-ethylenedioxythiophene/manganese oxide coated on porous carbon nanofibers as a potential anode for lithium-ion batteries. Energy Rep 2021;7:8677–87. https://doi.org/10.1016/j.egyr.2021.10.110.
[29] Alidoost M, Mangini A, Caldera F, Anceschi A, Amici J, Versaci D, et al. Micro-mesoporous carbons from cyclodextrin nanosponges enabling high-capacity silicon anodes and sulfur cathodes for lithiated Si-S batteries. Eur J Chem 2022;28:e202104201. https://doi.org/10.1002/chem.202104201.
[30] Devi AU, Divya K, Kaleekkal NJ, Rana D, Nagendran A. Tailored SPVdF-co-HFP/SGO nanocomposite proton exchange membranes for direct methanol fuel cells. Polymer 2018;140:22–32. https://doi.org/10.1016/j.polymer.2018.02.024.

[31] Mohammed HY, Farea MA, Ali ZM, Shirsat SM, Tsai M-L, Shirsat MD. Poly(N-methyl pyrrole) decorated rGO nanocomposite: a novel ultrasensitive and selective carbon monoxide sensor. Chem Eng J 2022;441:136010. https://doi.org/10.1016/j.cej.2022.136010.
[32] Safdari SM, Malekie S, Kashian S, Akbari M. Introducing a novel beta-ray sensor based on polycarbonate/bismuth oxide nanocomposite. Sci Rep 2022;12:2496. https://doi.org/10.1038/s41598-022-06544-6.
[33] Ullah MA, Seung K, Chang H. Flexible strain sensors for wearable applications fabricated using novel functional nanocomposites: a review. Compos Struct 2022;284:115214. https://doi.org/10.1016/j.compstruct.2022.115214.
[34] Tan J, Liu S, Luo J, Li H. Well-ordered polystyrene colloidal spheres for light addressable potentiometric sensor. Thin Solid Films 2020;716:138417. https://doi.org/10.1016/j.tsf.2020.138417.
[35] Li X, Zhang Y, Li M, Zhao Y, Zhang L, Huang C. Convex-meniscus-assisted self-assembly at the air/water interface to prepare a wafer-scale colloidal monolayer without overlap. Langmuir 2021;37:225–49. https://doi.org/10.1021/acs.langmuir.0c02851.
[36] Carpenter R, Macres D, Kwak J-G, Daniel K, Lee J. Fabrication of bioactive inverted colloidal crystal scaffolds using expanded polystyrene beads. Tissue Eng C Methods 2020;26:143–55. https://doi.org/10.1089/ten.tec.2019.0333.
[37] Ye X, Huang J, Zeng Y, Sun L-X, Geng F, Liu H-J, et al. Monolayer colloidal crystals by modified air-water interface self-assembly approach. Nanomaterials 2017;7:291. https://doi.org/10.3390/nano7100291.
[38] Cai Z, Liu YJ, Leong ESP, Teng J, Lu X. Highly ordered and gap controllable two-dimensional non-close-packed colloidal crystals and plasmonic–photonic crystals with enhanced optical transmission. J Mater Chem 2012;22:24668–75. https://doi.org/10.1039/C2JM34896A.
[39] Min WL, Jiang P, Jiang B. Large-scale assembly of colloidal nanoparticles and fabrication of periodic subwavelength structures. Nanotechnology 2008;19:475604. https://doi.org/10.1088/0957-4484/19/47/475604.
[40] Wu Y, Zhang C, Yuan Y, Wang Z, Shao W, Wang H, et al. Fabrication of wafer-size monolayer close-packed colloidal crystals via slope self-assembly and thermal treatment. Langmuir 2013;29:14017–23. https://doi.org/10.1021/la402652t.
[41] Adamczyk Z, Nattich-Rak M, Sadowska M, Michna A, Szczepaniak K. Mechanisms of nanoparticle and bioparticle deposition – kinetic aspects. Colloids Surf, A 2013;439:3–22. https://doi.org/10.1016/j.colsurfa.2012.12.060.
[42] Oćwieja M, Adamczyk Z. Controlled release of silver nanoparticles from monolayers deposited on PAH covered mica. Langmuir 2013;29:3546–55. https://doi.org/10.1021/la304855k.
[43] Karabasz A, Szuwarzyński M, Nowakowska M, Bzowska M, Lewandowska-Łańcucka J. Stabilization of liposomes with silicone layer improves their elastomechanical properties while not compromising biological features. Colloids Surf B Biointerfaces 2020;195:111272. https://doi.org/10.1016/j.colsurfb.2020.111272.
[44] Derjaguin BV, Muller VM, Toporov YP. Effect of contact deformations on the adhesion of particles. J Colloid Interface Sci 1975;53:314–26. https://doi.org/10.1016/0021-9797(75)90018-1.
[45] Lewandowska-Łańcucka J, Staszewska M, Szuwarzyński M, Zapotoczny S, Kepczynski M, Olejniczak Z, et al. Design and characterization of silicone micromaterials: a systematic study. Mater Des 2018;146:57–68. https://doi.org/10.1016/j.matdes.2018.03.010.
[46] Hinrichsen EL, Feder J, Jøssang T. Geometry of random sequential adsorption. J Stat Phys 1986;44:793–827. https://doi.org/10.1007/BF01011908.
[47] Miyake K. Elastic modulus of polystyrene film from near surface to bulk measured by nanoindentation using atomic force microscopy Appl. Phys Lett 2006;89. 031925. https://doi.org/10.1063/1.2234648.
[48] Torres JM, Stafford CM, Vogt BD. Impact of molecular mass on the elastic modulus of thin polystyrene films. Polymer 2010;51:4211–7. https://doi.org/10.1016/j.polymer.2010.07.003.